Corrosion Behavior of Detonation Gun Sprayed Al Coating on Sintered NFeB

Jizhao Ma, Xiaofang Liu, Wentao Qu, and Chungen Zhou

Pure Al coating was prepared by a detonation gun (D-gun) spraying process to protect sintered NdFeB magnets. The detonation gun sprayed coating is very uniform and has a low porosity of 0.77%. The thickness of the Al coating is approximately 16 μm. The corrosion current density for the coated sample was 1.30×10^{-5} A/cm^2 immediately after immersion in 3.5% NaCl solution, compared to 6.54×10^{-5} A/cm^2 for the uncoated sample. X-ray photoelectron spectrometry results indicate that the formation of Al$_2$O$_3$ film contributes to the increased corrosion resistance of Al coating. Meanwhile, electrochemical impedance spectroscopy with equivalent electrical circuit was used to ascertain the corrosion process of the Al coatings. Results show the corrosion procedure consists of two stages which agree with the potentiodynamic polarization test. It can be concluded that the Al coating deposited by the D-gun spray process can improve the corrosion resistance of sintered NdFeB.

Keywords	Al coating, corrosion resistance, detonation gun spraying

1. Introduction

NdFeB permanent magnets, with high strength of permanent magnetism, are far superior to all other types of magnets for a variety of engineering applications, including computer peripherals, automation, automobiles, aerodynamic, magnetic resonance, biomedical, acoustics and consumer electronics (Ref 1). Nowadays, sintered NdFeB magnets trend toward light weight, small thickness, short length, and small volume parts with the improvement of industrial requirements. However, the presence of electrochemically active phases in the microstructure of sintered NdFeB magnets diminishes their efficiency (Ref 2, 3). The Nd-rich phase is one of the active phases in sintered NdFeB magnets and preferential attack of this phase gives rise to intergranular corrosion, especially during exposure to humid and corrosive environments (Ref 4, 5).

Over the past few years, extensive research efforts have been directed to devise methods of improving their corrosion resistance, including alloy additions (Ref 6, 7) and surface coatings (Ref 8-12). Recently, the commonly used methods in industries are surface coatings technologies,

such as electroplating, electroless plating, and physical vapor deposition. Al coating is well suited for corrosion protection due to good performance, low costs and its dense oxide scale in the atmosphere. Shoudong Mao et al. (Ref 13-15) researched the corrosion behavior of Al coatings by direct current (DC) magnetron sputtering, and the effects of Ar$^+$ ion-beam-assisted deposition (IBAD) on the corrosion behavior of Al coatings. Their results showed Al coatings by both DC magnetron sputtering and IBAD can slightly enhance the anti-corrosion property. Nevertheless, these Al coatings present columnar structures and a number of defects which could result in premature failure of the coatings (Ref 15, 16). Nowadays, several researchers are showing great interest in spray coating. Ma et al. (Ref 17) found that Al coatings on NdFeB substrates deposited by a cold spray process were very dense and could provide long-term protection. However, the thick coatings (170 μm) on sintered NdFeB probably reduce the magnetic properties of the magnets and hinder their application. According to the industrial requirements, the anticorrosive coatings must be dense, uniform and well connected to the NdFeB substance. On the other hand, the coatings must have no effect on the magnetic property of sintered NdFeB. The maximum magnetic energy product (BH$_{max}$), which is the magnetostatic energy per unit volume, is an important parameter to measure the ability of the stored energy. A coating with 12 μm thickness could make the value of BH$_{max}$ decrease from 132.35 to 129.80 kJ/m^3, and lose $0.06T$ of the residual magnetism intensity (B_r) (Ref 18). Therefore, the coatings should be as thin as possible to guarantee the magnetic property of sintered NdFeB.

Detonation gun (D-gun) spraying is an alternative spray technology, which was originally patented by Union Carbide (now Praxair) in 1995 and developed independently in 1969 at the Institute of Materials Science, Kiev, Ukraine (Ref 19). The D-gun spraying process, with rarely low porosity, high bond strength, and controllable thickness, is extremely superior to other spray coating

Jizhao Ma, Xiaofang Liu, and **Chungen Zhou**, Department of Materials Science and Engineering, Beijing University of Aeronautics and Astronautics, Key Laboratory of Aerospace Materials and Performance (Ministry of Education), Beijing 100191, China; and **Wentao Qu**, School of Mechanical Engineering, Xi'an Shiyou University, Xi'an 710065, China. Contact e-mail: cgzhou@buaa.edu.cn.

processes (Ref 19-21). Furthermore, the D-gun spraying technology process has advanced technical equipment and first-class product line. However, no such studies have so far been carried out for the corrosion properties of D-gun sprayed Al coatings on NdFeB materials. In this paper, the D-gun spraying technique was used to deposit Al coatings on sintered NdFeB magnets. The specimens with and without coatings were subjected to the potentiodynamic polarization test, neutral salt spray (NSS) test and electrochemical impedance spectroscopy (EIS) with equivalent electrical circuit (EEC) to ascertain the corrosion behavior of the Al coatings. Meanwhile, x-ray photoelectron spectrometry was used to confirm the corrosion products.

2. Experimental Details

Sintered NdFeB magnets (N35; Yingkehongye, Beijing) with dimensions of 18 mm × 18 mm × 3 mm were degreased by acetone, dried in air, and then grit-blasted prior to deposition. All specimens were in the state of demagnetization.

Industrial pure aluminum powders (99.5 wt.%) were produced by a high pressure argon gas atomization method, then sieved according to conventional sieve analysis and divided into different size ranges. The as-atomized powders with particle size in the range of 20–60 μm were employed for spraying onto NdFeB substrates. Figure 1 presents the scanning electron microscope (SEM) morphology of the Al powders used as feedstock material.

Detonation gun spraying equipment ("Ob" D-gun, Russia) was used to produce Al coatings on sintered NdFeB. The spray gas was acetylene and oxygen, and the blanket gas was nitrogen. The detailed spraying parameters are listed in Table 1.

The phases of the Al powders and Al coating was characterized by x-ray powder diffraction (XRD; Model D/Max 2500PC; Rigaku, Japan) with Cu K_α radiation and nickel filter at 40 mA under a voltage of 40 kV. The specimens were scanned with a scan rate of 6°/min and a scan angle of 20°-90°. The surface morphology and composition of Al coatings was studied by scanning electron microscopy (SEM; JSM-6010LA; UK) with energy dispersive spectroscope (EDS; Oxford, UK). The porosity in the Al coatings was evaluated by using image analysis on a metallographic microscope (MM; WD-JX; Nanjing).

The corrosion behavior of the Al/NdFeB was investigated by potentiodynamic polarization and EIS with a CHI604A electrochemical working station in 3.5 wt.% NaCl solutions at 25 ± 3 °C. A classical three-electrode cell configuration was used with saturated calomel (SCE) as the reference and Pt plate as the counter electrode. An area of 1 cm^2 on the specimen was exposed. The EIS measurements were obtained with a signal amplitude of 5 mV in the frequency range from 10^5 to 10^{-2} Hz. In order to further study the corrosion features of the Al coating, potentiodynamic polarization and EIS plots after different immersion times were tested. The specimen without coating was experimented on as a contrast. Here, the software ZsimpWin was approached by simulating the EIS curves with EEC.

A NSS (GB/T10587-2006) test was also carried out to study the corrosion resistance of the specimens using a standard salt spray cabinet spraying NaCl solution (50 g/dm^3) at PH 6.8. The samples with and without coatings were exposed at the temperature of 35 ± 2 °C for 200 h to observed the evolution of the corrosion phenomena. The surface of each corroded specimen after the salt spray test was documented using a macro-digital camera.

X-ray photoelectron spectroscopy (XPS; Axis Ultra; Kratos Analytical, UK) was used to analyze the chemical state of the oxide films on the coatings. The C 1 s peak from carbon contamination at 284.8 eV was used as a reference to correct for charging shifts. The depth profiles were obtained by Argon ion bombardment with an ion energy of 2 kV over an area of 6 × 6 mm^2. The quantification of the species in the oxide films was performed via XPS peak 4.1 peak fitting software.

## 3. Results and Discussion

3.1 Structure and Composition

Figure 2 shows the XRD patterns of the atomized powders and D-gun spray deposited coatings. It is notable that a single Al phase with face-centered cubic (FCC)
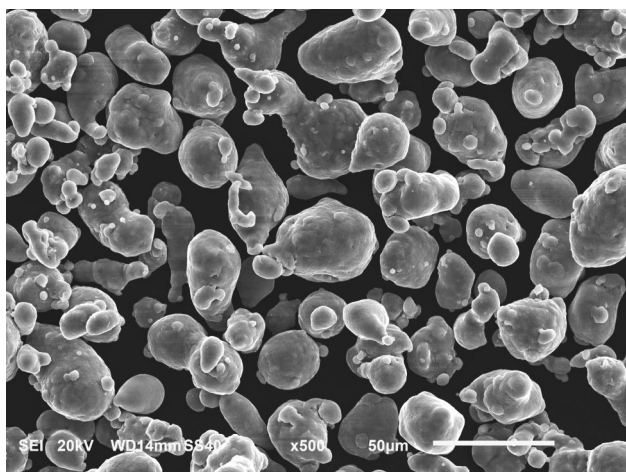
Fig. 1 SEM morphology of the Al powders used as feedstock material

Table 1 Process parameters for D-gun spray process

| Parameter	Related value
Fuel ratio (O_2/C_2H_2)	1.2
Powder feed rate, g/s	0.1
Spray distance, mm	120
Shot frequency, cycle/s	4
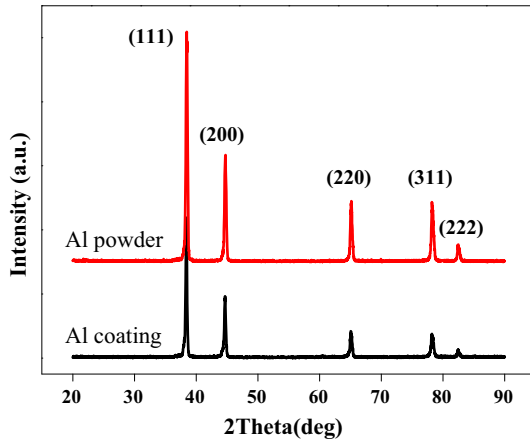
Fig. 2 XRD patterns of the Al powders and D-gun sprayed Al coating

crystal structure appears in both Al powders and Al coatings. It indicates that there is no obvious oxidation during the D-gun spraying process.

The micrographs of the surface and the cross-section of the Al coating on sintered NdFeB permanent magnets are revealed in Fig. 3. Compared with Fig. 1, it can be seen in Fig. 3a that the Al coating consists of flattenings, with almost uniform distribution. This is because particles were heated and partly melted in the spray gun, and were then sprayed onto the substrate rapidly (Ref 22). Meanwhile, there are small globular particles on the surface, which most probably are unmelted particles. Apparently, the coating has a dense layered structure with no cracks and defects in Fig. 3b. The thickness of the Al coating is approximately 16 μm. The interface of the NdFeB becomes irregular, which is due to the grit-blasting surface preparation before D-gun spraying. After the grit-blasting process, the half-molten particles with high velocity impinged against the target substrate, resulting in greater adhesion and hardness (Ref 23, 24). The coating surface has a low average porosity about 0.77% analyzed by metallographic microscope, which is typical of detonation-sprayed coatings (Ref 25, 26).

3.2 Potentiodynamic Curves Measurements

Figure 4a presents the potentiodynamic polarization curves of the Al coatings deposited by the detonation process with different immersion times in 3.5 wt.% NaCl solutions. In order to confirm the effect of the Al coatings, the NdFeB substance was tested as a contrast. It is clear that the anode sites of potentiodynamic polarization curves show the phenomenon of passivation when the NdFeB surfaces were deposited by Al coatings. Table 2 shows the corrosion potential (E_{corr}), corrosion current density (i_{corr}), cathodic Tafel slope (β_c) and anode Tafel slope (β_a) obtained from Fig. 4. The Tafel slope (β_c, β_a) represents the resistance of the relevant reaction. In our case, the anodic polarization of the Al-coated samples exhibit passivity. Thus, the cathodic branches can be extrapolated back to the corrosion potential E_{corr} to give
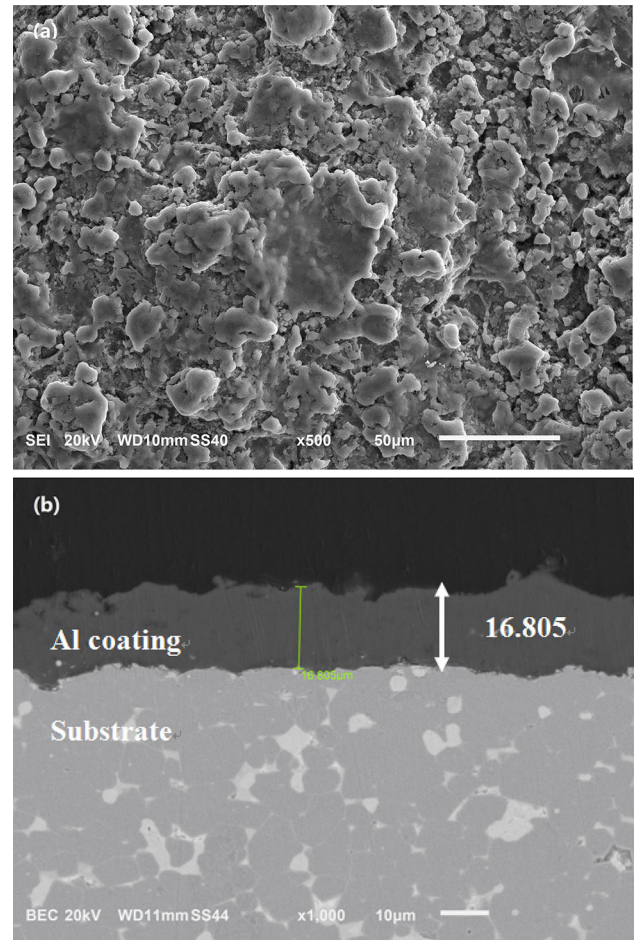

Fig. 3 SEM morphologies of the Al coating: (a) surface, (b) cross-section

the corrosion current density, i_{corr} (Ref 27). Figure 4b gives a representative example for such calculations, showing how to determine the values of E_{corr}, i_{corr}, β_c and β_a for the Al-coated samples. As seen in Table 2, the corrosion current density of the Al coatings is less than that of NdFeB (6.536×10^{-5} A/cm^2). The corrosion potential of NdFeB is obviously higher than that of the Al coating. That is attributed to a preferential corrosion of Al coatings when they are exposed to electrolyte simultaneously. The i_{corr} of the Al coating after immersion for 24 h is higher than that of the Al coating without immersion, and the E_{corr} of 24 h is more negative than that at the beginning of the immersion time. It is possible that the damage of the oxide film, which formed in the air, results in a greater corrosion tendency. As the immersion time grows, the i_{corr} of Al coating decreases. The Al coating after 48 h immersion (6.099×10^{-6} A/cm^2) has only one-tenth the i_{corr} of the sintered NdFeB substance. Meanwhile, the corrosion potential shifts toward a less negative value as the i_{corr} decreases. This may imply the formation of a new uniform oxidation film, which prevents solution ion penetration. Although the porosity of the Al coating prepared by D-gun spraying (0.77%) is lower than

that of the cold-spray coating (1.57%), the i_{corr} (1.301 × 10^{-5} A/cm^2) of the D-gun sprayed coating is larger (Ref 18). This is probably because the thick coating (170 μm) deposited by cold-spray could prevent penetration of solution ions.

The Al coating can play a sacrificed role when local defects of the coating occurs, therefore it could decrease the risk of coating application in a corrosion environment. Al coatings deposited by D-gun spraying, which have no cracks or defects, prevent the evolution of corrosion.
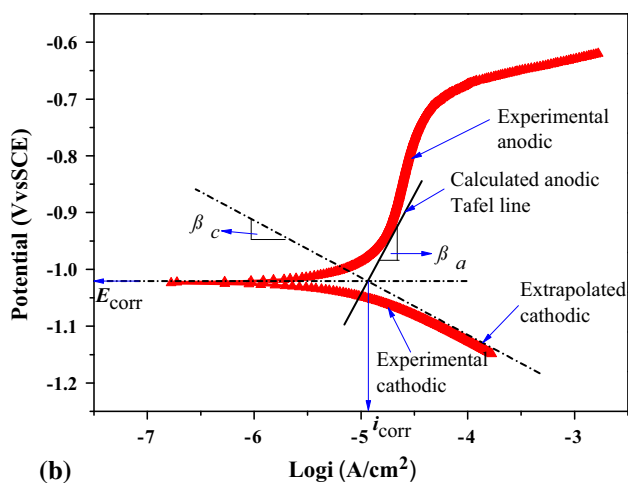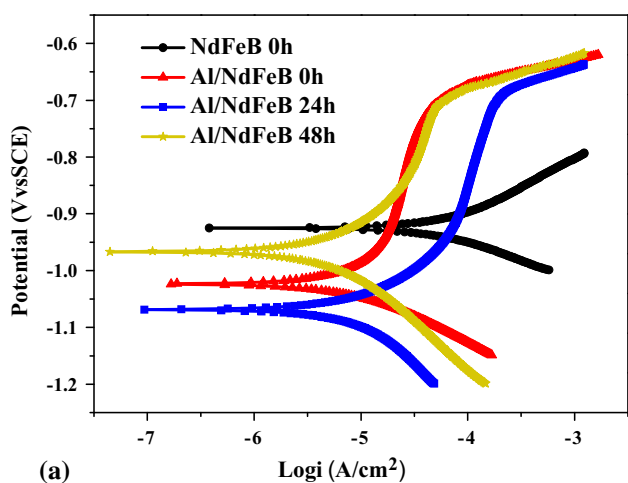
Fig. 4 (a) Potentiodynamic polarization curves obtained from NdFeB and Al coating with different immersion times in 3.5 wt.% NaCl solutions, (b) a representative example of calculating electrochemical parameters by using the Tafel extrapolation method

Moreover, the formation of a dense oxidation film further improves the corrosion resistance. That is to say, the Al coating prepared by D-gun spraying can provide excellent protection for sintered NdFeB magnets.

3.3 Neutral Salt Spray Test (NSS)

The optical photographs of the coated and uncoated specimens after 200 h NSS test are shown in Fig. 5. There is a little white rust formed on the surface of the Al coating (Fig. 5a). The white rust is probably the oxide film. However, the NdFeB is completely covered by the red rusty corrosion products (Fig. 5b). This indicates that Al-coated NdFeB can stand for 200 h against neutral 5.0 wt.% NaCl salt spray (35 ± 2 °C). The excellent corrosion resistance of Al coating deposited by D-gun spraying may be partly attributed to its well-known resistance to hot/wet environments compared with NdFeB magnets.

3.4 Electrochemical Impedance Spectroscopy (EIS) and Equivalent Electrical Circuit (EEC)

To further evaluate the corrosion behavior, the EIS of Al coatings and sintered NdFeB substrate in a 3.5 wt.% NaCl solutions were studied with different immersion times. Figure 6 presents the Nyquist diagrams of EIS. It can be observed that the Nyquist plot of NdFeB is a high capacitive loop followed by a low inductive loop, which is commonly associated with the charge transfer of the corrosion process and double-layer behavior at the coating–electrolyte interface (Ref 28-30). The low frequency inductive loop is typically due to the process whereby chloride ions absorb the substrate at the vulnerable region, indicating nucleation of corrosion pits. However, the Al coatings have only one high capacitive loop, which is attributed to electrolyte penetration including water uptake and salt intrusion (Ref 30, 31). As seen in Fig. 6, with the increase in the immersion, the diameter of the capacitance loop tends to shrink to start with, and then to enlarge with a diffusion loop appearing. Furthermore, the diameter of the capacitive loops in the Nyquist diagram is closely connected with the corrosion resistance. That is to say, the corrosion process of Al coatings consists of two stages, and both can provide more or less protection for NdFeB substrates.

In order to ensure the corrosion mechanisms in detail, the EIS results were analysed with ZSimpWin software using the EEC shown in Fig. 7. To accurately fit the EIS curves, a constant phase angle element (CPE; designated as Q) was introduced here to replace the pure capacitance.

Table 2 Electrochemical parameters calculated from the potentiodynamic curves in Fig. 4

Specimen	Immersion time, h	E_{corr}, V vs. SCE	i_{corr}, A/cm^2	β_c, V/dec	β_a, V/dec
NdFeB	0	−0.925	6.536 × 10^{-5}	0.070	0.096
Al/NdFeB	0	−1.024	1.301 × 10^{-5}	0.097	0.455
Al/NdFeB	24	−1.069	2.253 × 10^{-5}	0.189	0.316
Al/NdFeB	48	−0.967	6.099 × 10^{-6}	0.167	0.135
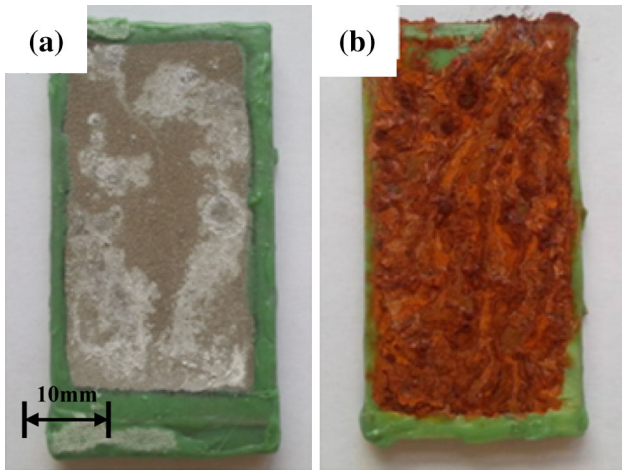
**Fig. 5** Optical photographs of (a) Al coating; and (b) NdFeB substrate after the 200-h NSS test
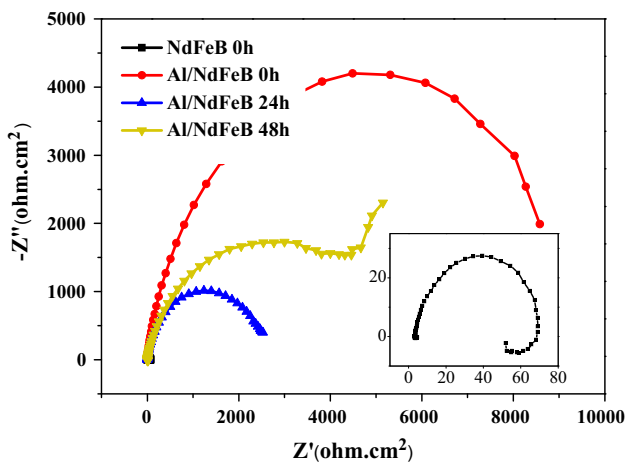
Fig. 6 Nyquist plots of the NdFeB and Al coating with different immersion times in 3.5 wt.% NaCl solutions

The admittance of CPE (Y_{CPE}) can be expressed by the following equation (Ref 30, 32):

$$Y_{CPE} = Q(j\omega)^n, \qquad (Eq\ 1)$$

where Q is the CPE constant, j the imaginary unit ($j^2 = -1$), ω the angular frequency, and n ($0 < n < 1$) an empirical exponent. When $n = 1$, Q becomes equivalent to a true capacitance concerned with an ideal capacitor. When $n = 0$, Q amounts to a resistance. When $n = 0.5$, Q becomes equivalent to Warburg impedance.

Figure 7a shows the model $R_s(Q_1(R_c(Q_2R_{ct})))$ (Ref 33-35) which is used to fit the Nyquist plot in the first stage (0-24 h). In EEC (1), R_s represents the electrolyte resistance, which determines the corrosion resistance of the coatings. Q_1 relates to coating capacitance, and R_c is the ionic conducting defect resistance. Q_2, which is in parallel with Faraday charge transfer resistance R_{ct}, represents the double-layer capacitance in the vulnerable
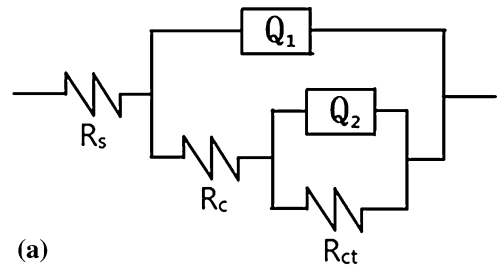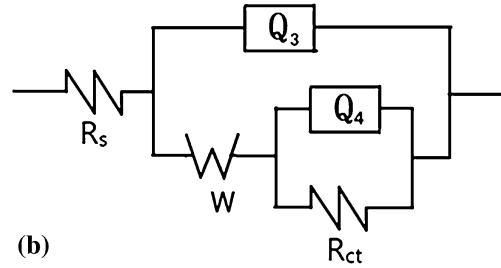
Fig. 7 Equivalent electrical circuits for EIS data in (a) the first stage, EEC (1) and (b) the second stage, EEC (2)

regions exposed to the bottom of the electrolyte penetration paths. The parameter values obtained for EEC (1) are tabulated in Table 3. It can be observed that both R_c and R_{ct} values decrease. This is because the chloride ions diffused through the pores and permeated to the surface of the metal particles at the first stage.

During the second corrosion stage (24-48 h), the EEC (2) of the Nyquist plots is given in Fig. 7b. In the $R_s(Q_3(W(Q_4R_{ct})))$ circuit, R_s, Q and R_{ct} represented solution resistance, constant phase element, and charge transfer resistance, respectively. Usually, Warburg impedance W may result from "finite-layer diffusion" or heterogeneous penetration of an electrolyte (Ref 36, 37). The simulated results are listed in Table 4. Obviously, the R_{ct} increased in this stage. The diffusion resistance agreed with the insulation of corrosion products which occurred because corrosion products cut off contact between the metal particles and the substrate (Ref 38). Moreover, the value of R_s increased significantly during this stage, while there was almost no change in the first stage. This may be due to a lower Al^{3+} in the revolution in this stage, as most of the Al^{3+} involved into the reaction formed oxidation products. From the two stages, it can be concluded that the Al coating firstly dissolved in the active state and then formed a new passivation film which to a certain extent prevented the chloride ions from diffusing. Consequently, the corrosion behavior of the Al coating is in accordance with the potentiodynamic polarization result.
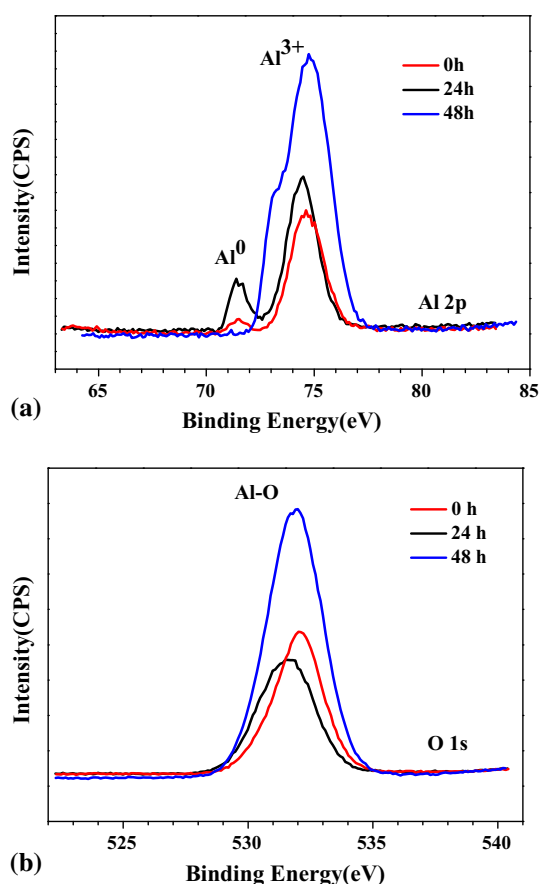
3.5 Corrosion Products

In order to accurately indentify the phase constitution formed on the coating surface, x-ray photoelectron spectrometry (XPS) was used. Figure 8 shows the XPS spectra of the Al coating after immersion for 0, 24, and 48 h in 3.5 wt.% NaCl solutions. The XPS spectra of Al 2p is

Table 3 Electrochemical parameters obtained from EEC in Fig. 7a by simulation

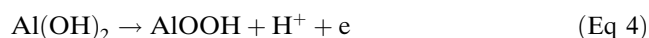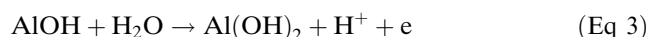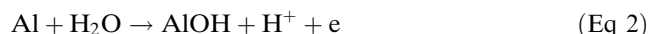| Specimen | Immersion time, h | R_s, Ω cm^2 | Q_1 | | | Q_2 | | | |
			$Y_0 - Q_1$, μS/cm^2 s^n	n	R_c, Ω cm^2	$Y_0 - Q_2$, μS/cm^2 s^n	n	R_{ct}, Ω cm^2
Al/NdFeB	0	1.57	18.49	0.9	1067	23	0.79	8781
Al/NdFeB	24	1.675	39.04	1	40.53	86.96	0.7755	2559

Table 4 Electrochemical parameters obtained from EEC in Fig. 7b by simulation

| Specimen | Immersion time, h | R_s, Ω cm^2 | Q_3 | | | Q_4 | | |
			$Y_0 - Q_3$, μS/cm^2 s^n	n	$Y_0 - W$, μS/cm^2 s^n	$Y_0 - Q_4$, μS/cm^2 s^n	n	R_{ct}, Ω cm^2
Al/NdFeB	48	14.77	34.55	1	1804	146.1	0.6333	4297

Fig. 8 XPS spectra of the Al coating after immersion in 3.5 wt.% NaCl solutions for 0, 24, and 48 h: (a) Al 2p, (b) O 1s

shown in Fig. 8a. This indicates that Al peaks of 0 h and 24 h decomposed into metallic Al and Al^{3+}, which was assigned to the binding energy (BE) of 71.5 $\pm$ 0.1 and 74.5 $\pm$ 0.2 eV, respectively (Ref [39, 40]). However, there is only one peak located at a BE of about 74.75 eV, in the Al 2p spectrum of 48 h. This is assigned to Al^{3+} in Al$_2$O$_3$/Al(OH)$_3$. It is difficult to identify the compound exactly because the peak positions of Al$_2$O$_3$ and Al(OH)$_3$ are

very close. Figure 8b displays the O 1 s core level spectra on the coating surface for different immersion times. The single signal at a BE of 531.7 $\pm$ 0.3 eV reveals a Al–O bond (Ref [41, 42]). According to the spectra of Al and O, the composition on the coating surface should be Al$_2$O$_3$. The formation of the oxide films on the Al coating in a NaCl solution can be expressed by the following equations (Ref [43]):

$$Al + H_2O \rightarrow AlOH + H^+ + e \qquad (Eq\ 2)$$

$$AlOH + H_2O \rightarrow Al(OH)_2 + H^+ + e \qquad (Eq\ 3)$$

$$Al(OH)_2 \rightarrow AlOOH + H^+ + e \qquad (Eq\ 4)$$

The overall reaction equation is Al + H$_2$O $\rightarrow$ AlOOH + 3H$^+$ + 3e, where AlOOH is Al$_2$O$_3$·H$_2$O. Furthermore, with immersion time extension, the concentration ratio of Al^{3+} is 1:0.86:1.36 tested by quantitative analysis of the XPS (Fig. 8b). That is to say, Al$_2$O$_3$ formed during preparation first dissolved and then re-formed. The forming process of Al$_2$O$_3$ proves that the corrosion mechanism of the Al coating has two stages, which is correspond to the EEC result. Therefore, Al$_2$O$_3$ acts as a barrier on the coating surface, which prevents further penetration of solution ions and improves the corrosion resistance of the Al coatings.

4. Conclusions

The Al powder could be successfully sprayed onto sintered NdFeB magnets by the D-gun spray process. The Al coating was uniform and dense, and had 0.77% porosity. The thickness of the Al coatings was about 16 μm. The results from the potentiodynamic polarization test, NSS test and EIS tests indicate that the Al coatings exhibit better corrosion resistance than the NdFeB substrate. Good corrosion resistance of the coating is attributed to the formation of a protective Al$_2$O$_3$ film. The detonation gun sprayed Al coating is expected to become a promising candidate to improve the corrosion resistance of sintered NdFeB magnets.

References

1. M. Sagawa, S. Fujimura, N. Togawa, H. Yamamoto, and Y. Matsuura, New Material for Permanent Magnets on a Base of Nd and Fe, *J. Appl. Phys.*, 1984, **55**, p 2083-2087
2. J. Jacobson and A. Kim, Oxidation Behavior of Nd-Fe-B Magnets, *Appl. Phys.*, 1987, **61**, p 3763-3765
3. L. Schultz, A.M. El-Aziz, G. Barkleit, and K. Mummert, Corrosion Behaviour of Nd-Fe-B Permanent Magnetic Alloy, *Mater. Sci. Eng. A*, 1999, **267**, p 307-313
4. I. Gurappa, Corrosion Characteristics of Permanent Magnets in Acidic Environments, *J. Alloys Compd.*, 2003, **360**, p 236-242
5. A.A. El-Moneim and A. Gebert, Electrochemical Characterization of Falvanically Coupled Single Phases An Nanocrystalline NdFeB-Based Magnets in NaCl Solutions, *J. Appl. Electrochem.*, 2003, **33**, p 795-805
6. L.Q. Yu, Y.H. Wen, and M. Yan, Effects of Dy and Nd on the Magnetic Properties An Corrosion Resistance of Sintered NdFeB, *J. Magn. Magn. Mater.*, 2004, **283**, p 353-356
7. H. Bala, G. Pawlowska, S. Szymura, V.V. Sergeev, and Y.M. Rabinovich, Corrosion Characteristics of Nd-Fe-B Sintered Magnets Containing Various Alloying Elements, *J. Magn. Magn. Mater.*, 1990, **87**, p L255-L259
8. T. Minowa, M. Yoshikawa, and M. Honshima, Improvement of the Corrosion Resistance on Nd-Fe-B Magnet with Nickel Plating, *IEEE Trans. Magn.*, 1989, **25**, p 3776-3778
9. C.W. Cheng, H.C. Man, and F.T. Cheng, Magnetic and Corrosion Characteristics of Nd-Fe-B Magnet with Various Surface Coatings, *IEEE Trans. Magn.*, 1997, **33**, p 3910-3912
10. Z. Chen, A. Ng, J.Z. Yi, and X.F. Chen, Muti-layered Electroless Ni-P Coatings on Powder-Sintered Nd-Fe-B Permanent Magnet, *J. Magn. Magn. Mater.*, 2006, **302**, p 216-222
11. N.C. Ku, C.-D. Qin, C.C. Yu, and D.H.L. Ng, Corrosion Resistance of NdFeB Magnets Coated by Al, *IEEE Trans. Magn.*, 1996, **32**, p 4407-4409
12. P. Mitchell, Corrosion Protection of NdFeB Magnets, *IEEE Trans. Magn.*, 1990, **26**, p 1933-1935
13. S.D. Mao, H.X. Yang, J.L. Li, H.G. Ying, and Z.L. Song, The Properties of Aluminium Coating on Sintered NdFeB by DC Magnetron Sputtering, *Vacuum*, 2011, **85**, p 772-775
14. S.D. Mao, H.X. Yang, Z.L. Song, J.L. Li, H.G. Ying, and K.F. Sun, Corrosion Behavior of Sintered NdFeB Deposited with an Aluminium Coating, *Corros. Sci.*, 2011, **53**, p 1887-1894
15. S.D. Mao, H.X. Yang, J.L. Li, F. Huang, and Z.L. Song, Corrosion Properties of Aluminium Coatings Deposited on Sintered NdFeB by Ion-Beam-Assisted Deposition, *Appl. Surf. Sci.*, 2011, **57**, p 5581-5585
16. A.R. Gonzalez-Elipe, F. Yubero, and J.M. Sanz, *Low Energy Ion Assisted Film Growth*, 1st ed., Imperial College Press, London, 2003
17. C.C. Ma, X.F. Liu, and C.G. Zhou, Cold-Sprayed Al Coating for Corrosion Protection of Sintered NdFeB, *J. Thermal Spray Technol.*, 2014, **23**, p 456-462
18. S.X. Yu and L. Chen, Preparation Technology and Performances of Zn-Cr Coating on Sintered NdFeB Permanent Magnet, *J. Rare Earths*, 2006, **24**, p 223-226
19. Y.A. Kharlamov, Detonation Spraying of Protective Coatings, *Mater. Sci. Eng.*, 1987, **93**, p 1-37
20. L. Byrnes and M. Kramer, Method and Apparatus for the Application of Thermal Spray Coatings onto Aluminium Engine Cylinder Bores, *Proceedings of the 7th National Thermal Spray Conference*, 1994 p 39-48
21. G. Kaushal, H. Singh, and S. Prakash, Comparative High Temperature Analysis of HVOF Sprayed and Detonation Gun Sprayed Ni-20Cr Coating in Laboratory and Actual Boiler Environments, *Oxid. Met.*, 2011, **76**(3-4), p 169-191
22. G. Sundararajan, D. Sen, and G. Sivakumar, The Tribological Behaviour of Detonation Sprayed Coatings: The Importance of Coating Process Parameters, *Wear*, 2005, **258**, p 377-391
23. J. Knapp, Fine-Particle Slurry Wear Resistance of Selected Tungsten Carbide Thermal Spray Coatings, *Tribol. Int.*, 1997, **30**(3), p 225-234
24. L. Pawlowski, *The Science and Engineering of Thermal Spray Coatings*, Wiley, West Susseex, 1995
25. B. Rajasekaran, S.G.S. Raman, S. Joshi, and G. Sundararajan, Influence of Detonation Gun Sprayed Alumina Coating on AA 6063 Samples Under Cyclic Loading With and Without Fretting, *Tribol. Int.*, 2008, **41**(4), p 315-322
26. N.K. Ramakrishna Naidu and S. Ganesh Sundara Raman, Effect of Shot Blasting on Plain Fatigue and Fretting Fatigue Behaviour of Al-Mg-Si Alloy AA6061, *Int. J. Fatigue*, 2005, **27**, p 323-331
27. E. McCafferty, Validation of Corrosion Rates Measured by the Tafel Extrapolation Method, *Corros. Sci.*, 2005, **47**, p 3202-3215
28. A.K. Singh and M.A. Quraishi, Effect of Cafazolin on the Corrosion of Mild Steel in HCl Solution, *Corros. Sci.*, 2010, **52**, p 152-160
29. C.-D. Qin, A.S.K. Li, and D.H.L. Ng, The Protective Coatings of NdFeB Magnets by Al and Al(Fe), *J. Appl. Phys.*, 1996, **79**, p 4854-4856
30. Q. Jiang, Q. Miao, W.P. Liang, F. Ying, F. Tong, Y. Xu, B.L. Ren, Z.J. Yao, and P.Z. Zhang, Corrosion Behavior of Arc Sprayed Al-Zn-Si-RE Coatings on Mild Steel in 3.5 wt.% NaCl Solution, *Electrochim. Acta*, 2014, **115**, p 644-656
31. J.G. He, J.B. Wen, and X.D. Li, Effects of Precipitates on the Electrochemical Performance of Al Sacrificial Anode, *Corros. Sci.*, 2011, **53**, p 1948-1953
32. J.F. Zhang, W. Zhang, C.W. Yan, K.Q. Du, and F.H. Wang, Corrosion Behaviors of Zn-Al-Mn Alloy Composite Coatings Deposited on Magnesium Alloy AZ31B (Mg-Al-Zn), *Electrochim. Acta*, 2009, **55**, p 560-571
33. I. Aziz, Q. Zhang, and M. Xiang, Using EIS to Evaluate Anticorrosion Properties of the $SiC_P/5A06$ Aluminium MMC Treated by Cerium Conversion Coatings, *J. Rare Earths*, 2010, **28**(1), p 109-116
34. E. Barsoulkov and J.R. Macdonald, *Impedance Spectroscopy Theory, Experiment, and Application*, 2nd ed., Wiley, Hoboken, NJ, 2005
35. J.M. Hu, J.Q. Zhang, and C.N. Cao, Determination of Water Uptake and Diffusion of Cl^- Ion in Epoxy Primer on Aluminum Alloys in NaCl Solution by Electrochemical Impedance Spectroscopy, *Prog. Org. Coat.*, 2003, **46**, p 273-279
36. X.H. Guo, K.Q. Du, Q.Z. Guo, Y. Wang, and F.H. Wang, Experimental Study of Corrosion Protection of a Three-Layer Film on AZ31B Mg Alloy, *Corros. Sci.*, 2012, **65**, p 367-375
37. S.A. Salman, R. Mori, R. Ichino, and M. Okido, Effect of Anodizing Potential on the Surface Morphology and Corrosion Property of AZ31 Magnesium Alloy, *Mater. Trans.*, 2010, **51**, p 1109-1113
38. L. Chen, N. Li, and D.R. Zhou, Corrosion Behavior of Sintered Zinc-Aluminum Coating in NaCl Solution, *Trans. Nonferrous Met. Soc. China*, 2002, **12**, p 1214-1217
39. N.M. Figueiredo, N.J.M. Carvalho, and A. Cavaleiro, An XPS Study of Au Alloyed Al-O Sputtered Coatings, *Appl. Surf. Sci.*, 2011, **257**, p 5793-5798
40. Yu.V. Plyuto, I.V. Babich, I.V. Plyuto, A.D. Van Langeveld, and J.A. Moulijn, XPS Studies of $MoO_3Al_2O_3$ and MoO_3SiO_2 Systems, *Appl. Surf. Sci.*, 1997, **119**, p 11-18
41. Q.D. Ling, S. Ling, E.T. Kang, K.G. Neoh, B. Liu, and W. Huang, Interface Formation Between the Al Electrode and Poly PFT Investigated In Situ by XPS, *Appl. Surf. Sci.*, 2002, **199**, p 74-82
42. N. Reddy, P. Bera, V. Rajagopal Reddy, N. Sridhara, A. Dey, C. Anandan, and A.K. Sharma, XPS Study of Sputtered Alumina Thin Films, *Ceram. Int.*, (in press)
43. S.Z. Song and Z.L. Tang, An Electrochemical Impedance Analysis on Aluminum in 3.5% NaCl Solution, *J. Chin. Soc. Corros. Prot.*, 1996, **16**, p 127-132